

Structure of a Surfactant-Templated Silicate Framework in the Absence of 3D Crystallinity

Niklas Hedin,^{†,‡} Robert Graf,[§] Sean C. Christiansen,[†] Christel Gervais,[#]
Ryan C. Hayward,^{†,‡} Juergen Eckert,^{‡,||} and Bradley F. Chmelka^{*,†,‡}

Contribution from the Department of Chemical Engineering, University of California, Santa Barbara, California, 93106, Materials Research Laboratory, University of California, Santa Barbara, California, 93106, Max-Planck-Institute für Polymerforschung, Postfach 3148, D-55021 Mainz, Germany, Los Alamos National Laboratory, Los Alamos, New Mexico 87545, and Laboratoire de Chimie de la Matière Condensée, Université Pierre et Marie Curie, CNRS-UMR 7574, 4 Place Jussieu, 75252 Paris CEDEX 05 France

Received January 29, 2004; E-mail: bradc@engineering.ucsb.edu.

Abstract: The structure of a novel molecularly ordered two-dimensional (2D) silicate framework in a surfactant-templated mesophase has been established by using a combination of solid-state nuclear magnetic resonance (NMR) spectroscopy, X-ray diffraction, and quantum chemical and empirical force-field modeling. These materials are unusual in their combination of headgroup-directed 2D crystalline framework ordering, zeolite-like ring structures within the layers, and long-range mesoscopic organization without three-dimensional (3D) atomic periodicity. The absence of registry between the silicate sheets, resulting from the liquidlike disorder of the alkyl surfactant chains, has presented significant challenges to the determination of framework structures in these and similar materials lacking 3D crystalline order. Double-quantum ²⁹Si NMR correlation experiments establish the interactions and connectivities between distinct intra-sheet silicon sites from which the structure of the molecularly ordered inorganic framework is determined.

Introduction

Solid-state NMR, in combination with energy minimization, provides the means to establish the structures of partially ordered solids, particularly those with high degrees of molecular order but lacking long-range atomic crystallinity. An interesting example is the family of lamellar surfactant-directed silicate mesophases with molecularly ordered inorganic frameworks.¹ Such framework ordering has been shown to depend on the structure-directing influences of strongly interacting surfactant headgroups, though disorder of the hydrophobic surfactant tails disrupts atomic registry between otherwise crystalline 2D silicate sheets.¹ In the absence of 3D crystalline order in these composites, determination of the atomic arrangements in the molecularly ordered frameworks has been challenging and not previously possible. Even for inorganic compounds with 3D crystalline registry between molecularly ordered sheets, it has proven difficult to grow the large crystals needed for single-crystal X-ray diffraction (XRD) structure determination. For example, of the more than 20 naturally occurring layered 3D

crystalline phyllosilicate minerals, only two, makatite² and silinaite,³ have to our knowledge had their structures solved by single-crystal XRD. Several phyllosilicates have been structurally analyzed by powder XRD methods, including kanemite,⁴ RUB-10,⁵ RUB-15,⁶ RUB-18,⁷ HLS,⁸ and AMH-3,⁹ all of which have 3D crystalline registry between their molecularly ordered sheets. In the absence of 3D atomic periodicity or when ordered domain dimensions are small, detailed determination of inorganic framework structures has been exceedingly difficult.

For the case of molecularly ordered silicate-alkylammonium surfactant mesophases (e.g., C₁₆N⁺Me₂Et, where Me represents a methyl group, Et is an ethyl moiety, and C₁₆ refers to a 16-carbon-atom alkyl chain), there is no 3D atomic registry between adjacent silicate sheets. Furthermore, the dimensions of the ordered domains are small (10–20 nm), as estimated from XRD and transmission electron microscopy (TEM). The mobile and disordered alkyl surfactant chains hinder molecular ordering

[†] Department of Chemical Engineering, University of California, Santa Barbara.

[‡] Materials Research Laboratory, University of California, Santa Barbara.

[§] Max-Planck-Institute für Polymerforschung.

^{||} Los Alamos National Laboratory.

[#] Laboratoire de Chimie de la Matière Condensée, Université Pierre et Marie Curie.

(1) Christiansen, S. C.; Zhao, D. Y.; Janicke, M. T.; Landry, C. C.; Stucky, G. D.; Chmelka, B. F. *J. Am. Chem. Soc.* **2001**, *123*, 4519–4529. Wang, L. Q.; Exarhos, G. J. *J. Phys. Chem. B* **2003**, *107*, 443–450.

(2) Annehed, H.; Falth, L.; Lincoln, F. J. *Z. Kristallogr.* **1982**, *159*, 203–210.

(3) Grice, J. D. *Can. Mineral.* **1991**, *29*, 363–367.

(4) Gies, H.; Marler, B.; Vortmann, S.; Oberhagemann, U.; Bayat, P.; Krink, K.; Rius, J.; Wolf, I.; Fyfe, C. *Micropor. Mesopor. Mater.* **1998**, *21*, 183–197.

(5) Gies, H.; Rius, J. *Z. Kristallogr.* **1995**, *210*, 475–480.

(6) Oberhagemann, U.; Bayat, P.; Marler, B.; Gies, H.; Rius, J. *Angew. Chem., Int. Ed. Engl.* **1996**, *35*, 2869–2872.

(7) Vortmann, S.; Rius, J.; Siegmann, S.; Gies, H. *J. Phys. Chem. B* **1997**, *101*, 1292–1297.

(8) Ikeda, T.; Akiyama, Y.; Izumi, F.; Kiyozumi, Y.; Mizukami, F.; Kodaira, T. *Chem. Mater.* **2001**, *13*, 1286–1295.

(9) Jeong, H. K.; Nair, S.; Vogt, T.; Dickinson, L. C.; Tsapatsis, M. *Nat. Mater.* **2003**, *2*, 53–58.

among the lamellar sheets and give rise to strong amorphous background X-ray scattering at wide angles, which obscures measurements of ordering over molecular length scales. As a consequence, it has not been possible to determine the structures of the highly ordered 2D-silicate frameworks in self-assembled silicate-surfactant mesophases using conventional scattering methods.

The development of powerful new techniques of solid-state NMR and molecular simulation, however, permit detailed structural analyses of complex molecularly ordered inorganic frameworks lacking 3D crystallinity, in this case a lamellar silicate-surfactant mesophase. By using 2D correlation ^{29}Si NMR techniques, the interconnectivities of five equally populated, tetrahedrally coordinated framework silicon sites (so-called T-sites) are unambiguously established. Out of a very large number of possible framework configurations, only one set of tetrahedrally coordinated Si site connectivities is consistent with the NMR measurements. With additional constraints imposed by small- and wide-angle XRD data, an energy-minimized structure was calculated using empirical force fields,¹⁰ as well as quantum chemical modeling.¹¹ These results were cross-validated by independent comparison with isotropic ^{29}Si NMR chemical shifts calculated from ab initio predictions, based on the minimum energy structure. This allows, for the first time, inorganic framework structures to be determined in the absence of 3D order, here, the 2D-crystalline silicate sheets in a surfactant-templated mesophase.

Experimental Section

Lamellar silicate- $\text{C}_{16}\text{N}^+\text{Me}_2\text{Et}$ surfactant mesophases were synthesized by combining an aqueous solution containing 0.69 mmol dimethylethylhexadecylammonium bromide (ACROS 99%) in 83.7 mmol water, with a separate alkaline solution containing highly charged silica anions that were enriched in ^{29}Si (50%) to enhance NMR signal sensitivity. The alkaline silicate solution was prepared by dissolving 0.58 mmol $\text{SiO}_2(\text{s})$ enriched 95.65% (Oak Ridge National Laboratory) in ^{29}Si and 0.54 mmol SiO_2 (ACROS CAB-O-SIL M5 scintillation grade) in 11.1 mmol methanol, 18.8 mmol water, and 1.24 mmol tetramethylammonium hydroxide. The combined solution had an initial pH of ~ 12.5 , which was subsequently reduced to ~ 11.5 by the addition of concentrated HBr, leading to the formation of a white precipitate. The precipitate was annealed in its mother liquor at 135 °C in a Teflon-lined stainless steel autoclave for 23 days, after which it was washed with distilled water twice, filtered, and dried.

The resulting powder sample was characterized by X-ray diffraction on a Scintag X2 powder diffractometer with $\text{Cu } K_\alpha$ radiation (1.54 Å) over a range of 2θ angles from 1° to 35° in increments of 0.05°. Transmission electron microscopy (TEM) measurements were conducted using a JEOL 2010 HR microscope operating at 200 kV.

Solid-state ^{29}Si NMR spectra were acquired on a Bruker AVANCE-500 spectrometer operating at 99.35 MHz using an 11.7-T widebore magnet. Two-dimensional (2D) dipole-dipole-mediated Double-Quantum (DQ) $^{29}\text{Si}\{^{29}\text{Si}\}$ NMR spectra were acquired under conditions of magic-angle spinning (MAS) at 12.5 kHz at room temperature using a 4-mm probehead. Although dipolar interactions are in general averaged under fast MAS conditions, they are reintroduced in the DQ experiment by rotor-synchronized radio frequency (rf) pulses that are applied stroboscopically. ^{29}Si signal sensitivity was enhanced and otherwise long $^{29}\text{Si } T_1$ relaxation times were circumvented by cross-polarization of ^1H magnetization to nearby ^{29}Si nuclei; the amplitude

of the ^1H radio frequency field was ramped between 80 and 100% of its maximum value. Sixty-four acquisitions were recorded for each of the 144 t_1 increments using a 2-s repetition delay; the $^1\text{H } T_1$ relaxation times were approximately 400 ms. Dipole-dipole interactions were reintroduced by 1.6-ms rotor-synchronized BABA¹² composite rf-pulses with rf-field strengths of 100 kHz, and TPPM¹³ decoupling was applied during the acquisition and the dipole-dipole recoupling periods.

The ^{29}Si NMR dipole-dipole interaction strengths (D) and their corresponding ^{29}Si -O- ^{29}Si distances (r) were determined from spinning-sideband-analyses¹⁴ of dipole-dipole-mediated 2D DQ $^{29}\text{Si}\{^{29}\text{Si}\}$ MAS NMR spectra. These NMR spectra were acquired on a Bruker DMX-300 NMR spectrometer operating at 59.64 MHz under conditions of MAS at 5 kHz at room temperature using a 4-mm probehead. ^{29}Si dipole-dipole interactions were reintroduced using rotor-synchronized BABA composite rf-pulses with rf-field strengths of 50 kHz and a 3.2-ms mixing time period together with non-rotor synchronized t_1 -increments.

Two-dimensional ^{29}Si MAS NMR anisotropic-isotropic chemical shift correlation spectra were acquired under MAS conditions with sample rotation frequencies (f) of 3 and 5 kHz on a Bruker DSX-500 spectrometer. Cross-polarization of ^1H magnetization was used for sensitivity enhancement. The NMR experiment "Separation of Undistorted Powder patterns by Effortless Recoupling (SUPER)",¹⁷ a modification of an NMR technique developed by Tycko et al.,¹⁸ was used to separate anisotropic and isotropic ^{29}Si chemical shifts. By applying blocks of 360° pulses symmetrically distributed within each rotor period, the ^{29}Si chemical shift anisotropy (CSA) was partially reintroduced. Although the ^{29}Si CSA line shape was preserved, its quasi-static spectrum was narrowed. The scaling between the recorded spectrum and the static spectrum can be described analytically and depends on the ^{29}Si rf-field strength and the MAS spinning speed.^{17,18} The 1D anisotropic ^{29}Si line shapes for the five different silicate sites were obtained from projections of the SUPER ^{29}Si NMR spectrum onto the anisotropic frequency axis after scaling. In the SUPER NMR experiment, the ^1H rf-field strength was $25 \cdot f$, and the ^{29}Si rf-field strength was $12.12 \cdot f$, the latter corresponding to a scaling factor of 0.15.¹⁷ The 5-kHz MAS experiments were performed with a 2.5-mm MAS probehead, which provided higher ^1H rf-field strengths, while the 3-kHz experiments used a 4-mm probehead, which provided more stable and precise sample spinning at lower MAS speeds.

Two-dimensional J -coupling-mediated $^{29}\text{Si}\{^{29}\text{Si}\}$ NMR spectra were acquired under MAS conditions at 8 kHz at room temperature using a mixing time of 9.6 ms. (This experiment is also referred to as the so-called "Incredible Natural Abundance Double Quantum Transfer Experiment," and by its acronym INADEQUATE.)^{15,16} The mixing time was optimized by maximizing integrated ^{29}Si signal intensity in a series of 1D J -coupling-mediated ^{29}Si NMR spectra. A phase cycle appropriate for the selection of DQ signals¹⁶ was used, and TPPM decoupling (50 kHz) was applied during the acquisition and the J -evolution time periods. The ^{29}Si 90° pulse length was 3.3 μs , and sixty-four acquisitions were recorded for each of the 96 t_1 increments using a 2-s repetition delay.

Empirical energy minimizations of the molecularly ordered silicate framework structure were performed using the GULP¹⁰ code and ab initio quantum molecular dynamics using VASP.¹¹ GULP uses a widely

(10) GULP (the General Lattice Utility Program) written and developed by J. D. Gale, Curtin University of Technology, Perth, Australia.
 (11) Kresse, G.; Furthmüller, J. *Comput. Mater. Sci.* **1996**, *6*, 15–50.

(12) Feike, M.; Demco, D. E.; Graf, R.; Gottwald, J.; Hafner, S.; Spiess, H. W. *J. Magn. Res. Ser. A* **1996**, *122*, 214–221.
 (13) Bennett, A. E.; Rienstra, C. M.; Auger, M.; Lakshmi, K. V.; Griffin, R. G. *J. Chem. Phys.* **1995**, *103*, 6951–6958.
 (14) Graf, R.; Demco, D. E.; Gottwald, J.; Hafner, S.; Spiess, H. W. *J. Chem. Phys.* **1997**, *106*, 885–895.
 (15) Lesage, A.; Emsley, L. *J. Magn. Reson.* **2001**, *148*, 449–454.
 (16) Lesage, A.; Auger, C.; Caldarelli, S.; Emsley, L. *J. Am. Chem. Soc.* **1997**, *119*, 7867–7868.
 (17) Liu, S. F.; Mao, J. D.; Schmidt-Rohr, K. *J. Magn. Reson.* **2002**, *155*, 15–28.
 (18) Tycko, R.; Dabbagh, G.; Mirau, P. A. *J. Magn. Reson.* **1989**, *85*, 265–274.

applied¹⁹ force-field for silicates and includes a shell-model representation for the non-hydroxyl oxygen atoms. The ab initio minimization with VASP¹¹ uses plane wave basis sets on a periodic lattice and interactions between ions and electrons described by pseudo-potentials. The *a*- and *b*-axis spacings were fixed to 0.85 and 0.68 nm, as established by wide-angle XRD data. An arbitrary (and insensitive) *c*-axis spacing of 1.75 nm was used to separate the silicate sheets, instead of ~ 3.5 nm as established by small-angle XRD, due to the difficulty of explicitly modeling the surfactant species, particularly the disordered alkyl chains and for reasons of computational efficiency.

Isotropic ²⁹Si NMR chemical shifts for silicon T-sites in the energy-minimized structure were calculated by using density functional theory, specifically the PARATEC code²⁰ with periodic boundary conditions. The GIPAW method²¹ ensures a reliable prediction of isotropic chemical shifts by using computationally efficient pseudo-potentials. The ²⁹Si chemical shift scale was normalized, so that experimental and theoretical isotropic chemical shifts for quartz coincide.²²

Results and Discussion

Solid-state NMR interactions are sensitive to local nuclear environments, yielding information on molecular structures and ordering which complements that available from scattering methods, particularly for poorly ordered systems.^{23,24} ‘NMR crystallography’ has been applied to crystalline solids to measure molecular or orientational ordering²⁵ and used to make detailed refinements of crystal structures,^{26–28} as well as to study phase transitions.²⁹ Recent methodological advances in solid-state NMR spectroscopy exploit homonuclear through-bond *J*-couplings or through-space dipole–dipole couplings, allowing detailed information on local bonding geometries and distances to be obtained.^{14,30–35} This is especially useful for systems lacking the long-range 3D atomic order that is typically required for structure determinations using diffraction methods. Such is the case for the lamellar silicate–C₁₆N⁺Me₂Et mesophase depicted schematically in Figure 1. This system has been shown to have a molecularly ordered silicate framework possessing five well-defined tetrahedrally coordinated silicon sites with 1:1:1:1:1 populations, as evidenced by five narrow (<1 ppm) ²⁹Si NMR peaks under conditions of MAS, and lamellar mesoscopic ordering, as established by SAXS.¹ Furthermore, by correlating

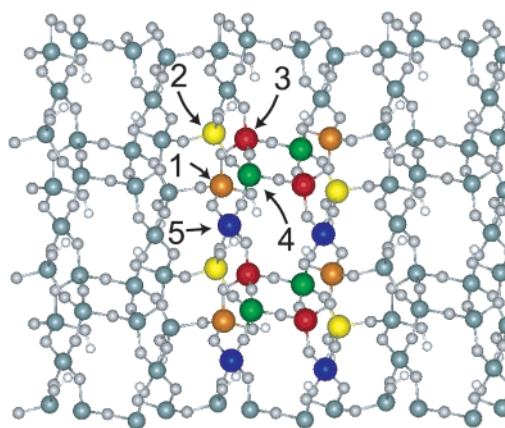
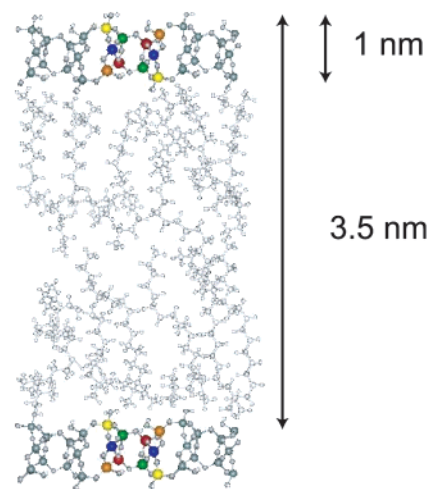


Figure 1. Energy-minimized structure of the molecularly ordered silicate sheets in the lamellar silicate–C₁₆N⁺Me₂Et mesophase. (a) Side-view, showing the layered structure in profile. The alkyl chains of the surfactant are disordered; their positions are not exact. (b) Top-view of the 2D silicate framework showing four- and six-membered silicate rings. The five different tetrahedrally coordinated silicon sites are highlighted, and the surfactant molecules are excluded for clarity. Two of the silicon sites are incompletely condensed *Q*³ species, site 1 (orange) and site 2 (yellow), while site 3 (red), site 4 (green), and site 5 (blue) are fully condensed *Q*⁴ moieties. The various Si sites correspond to the respectively labeled peaks in the 1D ²⁹Si MAS NMR spectrum of Figure 2.

- (19) Henson, N. J.; Cheetham, A. K.; Gale, J. D. *Chem. Mater.* **1996**, *8*, 664–670.
 (20) PARATEC (PARAllel Total Energy Code) by Pfrommer, B.; Raczowski, D.; Canning, A.; Louie, S. G.; Lawrence Berkeley National Laboratory (with contributions from Mauri, F.; Cote, M.; Yoon, Y.; Pickard C. and Heynes, P.) for more information see www.nersc.gov/projects/paratec.
 (21) Pickard, C. J.; Mauri, F. *Phys. Rev. B* **2001**, *63*, 245101.
 (22) Profeta, M.; Mauri, F.; Pickard, C. J. *J. Am. Chem. Soc.* **2003**, *125*, 541–548.
 (23) Eckert, H. *Prog. Nucl. Magn. Reson. Spectrosc.* **1992**, *24*, 159–293.
 (24) Laws, D. D.; Bitter, H. M. L.; Jerschow, A. *Angew. Chem., Int. Ed. Engl.* **2002**, *41*, 3096–3129.
 (25) Tycko, R.; Dabbagh, G. *J. Am. Chem. Soc.* **1991**, *113*, 3592–3593.
 (26) Taulelle, F.; Samoson, A.; Loiseau, T.; Ferey, G. *J. Phys. Chem. B* **1998**, *102*, 8588–8598.
 (27) Beitone, L.; Huguenard, C.; Gansmuller, A.; Henry, M.; Taulelle, F.; Loiseau, T.; Ferey, G. *J. Am. Chem. Soc.* **2003**, *125*, 9102–9110.
 (28) Fyfe, C. A.; Lewis, A. R.; Chezeau, J. M.; Grondy, H. *J. Am. Chem. Soc.* **1997**, *119*, 12210–12222.
 (29) Liu, S. X.; Welch, M. D.; Klinowski, J. *J. Phys. Chem. B* **1997**, *101*, 2811–2814.
 (30) Lee, Y. K.; Kurur, N. D.; Helmle, M.; Johannessen, O. G.; Nielsen, N. C.; Levitt, M. H. *Chem. Phys. Lett.* **1995**, *242*, 304–309.
 (31) Baldus, M. *Prog. Nucl. Magn. Reson. Spectrosc.* **2002**, *41*, 1–47.
 (32) Fyfe, C. A.; Grondy, H.; Feng, Y.; Kokotailo, G. T. *Chem. Phys. Lett.* **1990**, *173*, 211–215.
 (33) Feike, M.; Graf, R.; Schnell, I.; Jäger, C.; Spiess, H. W. *J. Am. Chem. Soc.* **1996**, *118*, 9631–9634.
 (34) Schmidt-Rohr, K. *Macromolecules* **1996**, *29*, 3975–3981.
 (35) Sakellariou, D.; Brown, S. P.; Lesage, A.; Hediger, S.; Bardet, M.; Meriles, C. A.; Pines, A.; Emsley, L. *J. Am. Chem. Soc.* **2003**, *125*, 4376–4380.

natural abundance 2D ²⁹Si{²⁹Si} MAS NMR signal intensities mediated by through-bond *J*-coupling interactions, interconnectivities among the five tetrahedral sites (T-sites) were established, although incompletely so. For the reasons discussed above, and because ²⁹Si–O–²⁹Si *J*-couplings cannot distinguish interactions between multiple like sites, the interconnectivities among the framework T-sites could not be fully specified. Thus, the structure has remained indeterminate.

Historical obstacles to the determination of difficult framework structures can be overcome by exploiting recent advancements^{14,15} in ‘NMR crystallography’. The ²⁹Si nuclei in layered silicate frameworks lend themselves especially well to such approaches, as their solid-state ²⁹Si MAS NMR spectra generally yield well-resolved ²⁹Si peaks from distinct Si sites.³⁶ An advantageous approach is to exploit through-space homonuclear dipole–dipole-coupling interactions, which are generally stronger and longer-range than weaker through-bond *J*-coupling

- (36) Lippmaa, E.; Magi, M.; Samoson, A.; Engelhardt, G.; Grimmer, A. R. *J. Am. Chem. Soc.* **1980**, *102*, 4889–4893.

interactions. Pairwise ^{29}Si –O– ^{29}Si dipole–dipole couplings are measured in a 2D Double-Quantum (DQ) $^{29}\text{Si}\{^{29}\text{Si}\}$ MAS NMR experiment to establish spatial proximities of nearest-neighbor and next-nearest-neighbor T-sites. Because the ^{29}Si dipole–dipole correlations between next-nearest-neighbor T-sites are weak, it is helpful to partially enrich the silicate frameworks in ^{29}Si (from 4.7% at natural abundance to $\sim 50\%$). This increases the concentration of ^{29}Si –O– ^{29}Si spin pairs and, importantly, enhances the sensitivity of the 2D DQ ^{29}Si NMR measurements.

On the basis of the DQ ^{29}Si NMR correlations measured (positions and intensities), it is possible to establish which ^{29}Si nuclei occupy nearest-neighbor T-sites, linked through bridging covalently bonded oxygen atoms,^{1,32} and which ^{29}Si framework sites are more distant, though still interacting through distance- (and mobility-) dependent dipole–dipole interactions.³⁷ Dipole–dipole interactions permit double-quantum ^{29}Si states to be created, with each DQ ^{29}Si chemical shift corresponding to the sum of the chemical shifts of the two individual ^{29}Si nuclei in a given dipole–dipole-coupled spin pair. By reintroducing the dipole–dipole interaction and with appropriate phase cycling, the intensities among the DQ and single-quantum ^{29}Si chemical shifts can be correlated to identify different framework Si site connectivities and to distinguish nearest and next-nearest T-site neighbors among the interacting ^{29}Si spin pairs.

Figure 2, for example, shows a dipole–dipole-mediated 2D DQ ^{29}Si MAS NMR spectrum for a molecularly ordered silicate– $\text{C}_{16}\text{N}^+\text{Me}_2\text{Et}$ lamellar mesophase with clearly evident signal correlations that can be categorized unambiguously both by type and intensity. The strong ‘off-diagonal’ intensities in the spectrum correspond to DQ ^{29}Si signals that are correlated to two different ^{29}Si sites at their respective chemical shifts, which establishes that the different pairs of distinct ^{29}Si sites are in close spatial proximities. Similarly, ‘diagonal’ signal intensity, in which a single peak appears with a DQ shift that is twice that of the corresponding chemical shift, reflects the close proximity of chemically and structurally identical sites. Framework site connectivities are established by assigning the strongest intensities in Figure 2 to neighboring ^{29}Si –O– ^{29}Si sites (0.26–0.33 nm)³⁸ and by taking into account that ^{29}Si sites 1 and 2 are incompletely condensed Q^3 species and that sites 3, 4, and 5 are fully condensed Q^4 species, the number densities of all five sites being identical. (Q^n represents a tetrahedrally coordinated silicon site, with n nearest-neighbor –O–Si–moieties.) The integral intensities of the five narrow, well resolved peaks in the one-pulse ^{29}Si MAS NMR spectrum in Figure 2 are the same.

The silicon T-site assignments are based on known ^{29}Si chemical shift ranges, ^1H -to- ^{29}Si cross-polarization properties,¹ and are validated separately by correlating isotropic and anisotropic ^{29}Si MAS NMR line shapes.¹⁷ Figure 3 shows 1D ^{29}Si chemical-shift-anisotropy (CSA) line shapes that are associated with each of the five different silicate framework sites, as obtained from projections onto the anisotropic axis of a 2D ^{29}Si MAS NMR anisotropic–isotropic correlation spectrum. The broad powder line shapes associated with sites 1 and 2 are characteristic of the reduced symmetries of Q^3 ^{29}Si T-sites, compared to the narrower line shapes from the more condensed

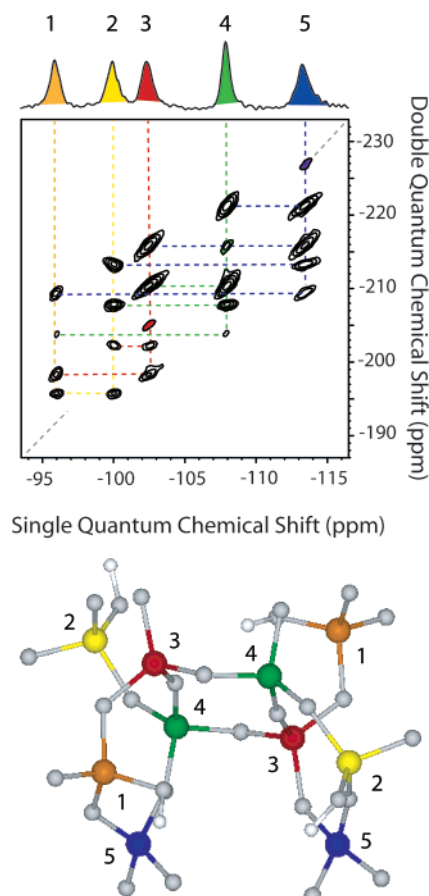


Figure 2. Dipole–dipole-mediated 2D Double-Quantum $^{29}\text{Si}\{^{29}\text{Si}\}$ MAS NMR spectrum from a lamellar silicate– $\text{C}_{16}\text{N}^+\text{Me}_2\text{Et}$ mesophase with a molecularly ordered framework, enriched 50% in ^{29}Si . A single-pulse ^{29}Si MAS NMR spectrum, with five resolved peaks of equal 1:1:1:1:1 integral intensities accompanies the contour plot along the horizontal single-quantum dimension, while the double-quantum dimension lies along the vertical axis. Spatial proximities between pairs of dipole–dipole-coupled ^{29}Si sites are established by correlated ^{29}Si signal intensities at identical double-quantum, chemical shifts. The lowest contour level is at 4% of the full intensity, and each new level corresponds to an intensity increase by a factor of 2. The molecular building unit from which the ordered silicate framework is constructed (see discussion below) accompanies the spectrum.

and symmetric Q^4 framework moieties (sites 3, 4, and 5). These differences can be quantified by line shape fits to the spectra (Figure 3), from which the ^{29}Si CSA tensor elements are established. The values determined in this manner were $\{\sigma_{11}, \sigma_{22}, \sigma_{33}\} = \{-156, -71, -61\}$ ppm for site 1, $\{-144, -83, -73\}$ ppm for site 2, and $\{-112.5, -98.5, -98.5\}$ ppm for site 3. The CSA tensor elements determined by line shape fitting correspond to ^{29}Si chemical shift anisotropies³⁹ (δ) of 60 and 40 ppm for Q^3 sites 1 and 2, respectively, and 10 ppm for Q^4 site 3.⁴⁰ The narrow and symmetric ^{29}Si line shapes in Figure 3 for sites 4 and 5 precluded accurate determination of the CSA tensor elements for these sites. Instead, the line widths of the peaks in the anisotropic ^{29}Si frequency dimension were determined, yielding full-width-at-half-maximum values of 13 and 10 ppm for sites 4 and 5, respectively. The two ^{29}Si Q^3 sites

(37) Olivier, L.; Yuan, X.; Cormack, A. N.; Jäger, C. *J. Non-Cryst. Solids* **2001**, *293*, 53–66.

(38) Hench, L. L.; West, J. K. *Annu. Rev. Mater. Sci.* **1995**, *25*, 37–68.

(39) The magnitude and asymmetry of a given CSA tensor are expressed by the anisotropy parameter, $\delta = (\sigma_{11} - \sigma_{\text{iso}})$, and the asymmetry parameter, $\eta = (\sigma_{22} - \sigma_{33})/\delta$, respectively, with principal CSA-tensor elements (σ_{ij}) $\sigma_{11} < \sigma_{22} < \sigma_{33}$ and the isotropic chemical shift $\sigma_{\text{iso}} = (\sigma_{11} + \sigma_{22} + \sigma_{33})/3$.

(40) The relatively large chemical shift anisotropies of Q^3 sites 1 and 2 also account for the comparatively low ^{29}Si DQ signal intensities associated with these moieties.

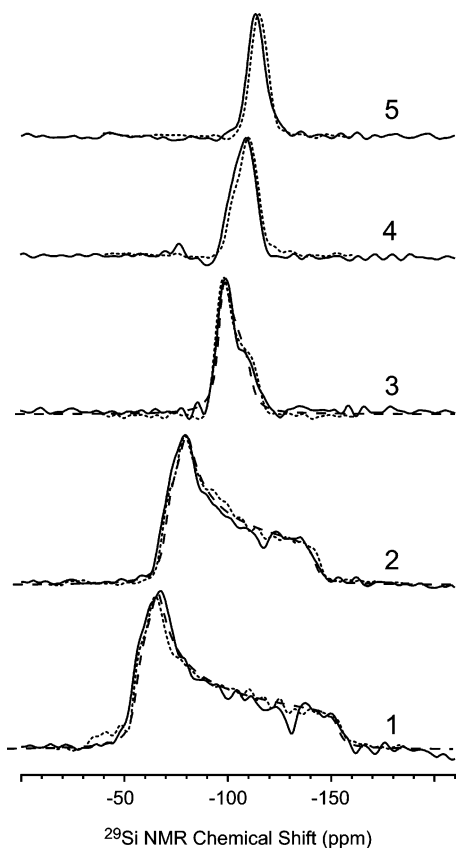


Figure 3. 1D ^{29}Si NMR spectra obtained from projections onto the anisotropic axis of a 2D anisotropic-isotropic correlation ^{29}Si MAS NMR spectrum acquired at room-temperature spinning at 3 kHz (dotted lines) or 5 kHz (solid lines) for the same lamellar silicate- $\text{C}_{16}\text{N}^+\text{Me}_2\text{Et}$ mesophase of Figure 2. The broad line shapes associated with sites 1 and 2 confirm them to be Q^3 -type moieties, while the narrow spectra associated with sites 3, 4, and 5 show these to be Q^4 -type moieties. Chemical-shift-anisotropy (CSA) line shape fits (dashed lines) accompany spectra 1, 2, and 3, from which chemical shift tensor elements are estimated: site 1 $\{\sigma_{11}, \sigma_{22}, \sigma_{33}\} = \{-156, -71, -61\}$ ppm; site 2 $\{\sigma_{11}, \sigma_{22}, \sigma_{33}\} = \{-144, -83, -73\}$ ppm; site 3 (width comparable also to sites 4 and 5) $\{\sigma_{11}, \sigma_{22}, \sigma_{33}\} = \{-112.5, -98.5, -98.5\}$ ppm.

have nonzero asymmetry parameters of $\eta = 0.16$ and 0.23 , respectively, reflecting their less symmetric electron distributions. For each of the three ^{29}Si Q^4 moieties, $\eta \approx 0$, as expected. These measurements unambiguously establish the reduced symmetries and large chemical shift anisotropies that are characteristic of Q^3 sites 1 and 2, compared to Q^4 sites 3, 4, and 5.

Once the Q^3 and Q^4 designations for the five framework Si sites are known, the intraframework connectivities for sites 1, 2, and 5 are readily determined from the correlated signal pairs in J -coupling- and dipole-dipole-mediated double-quantum 2D $^{29}\text{Si}\{^{29}\text{Si}\}$ MAS NMR spectra. In particular, the 2D INADEQUATE $^{29}\text{Si}\{^{29}\text{Si}\}$ MAS NMR spectrum of Figure 4 reflects J -mediated interactions between nearest-neighbor $^{29}\text{Si}-\text{O}-^{29}\text{Si}$ T-sites. For example, signal intensities associated with Q^3 site 1 are correlated with signals from sites 2, 3, and 5, whereas the other Q^3 site 2 displays signal correlations with sites 1, 4, and 5. Thus, the local framework interconnectivities of Q^3 sites 1 and 2 (each bonded to three other $-\text{O}-\text{Si}$ nearest neighbor species) are fully specified; a terminal $-\text{O}^-$ must also be associated with each of these Q^3 moieties, charge-compensated by either a proton (as a silanol species, $-\text{OH}$) or

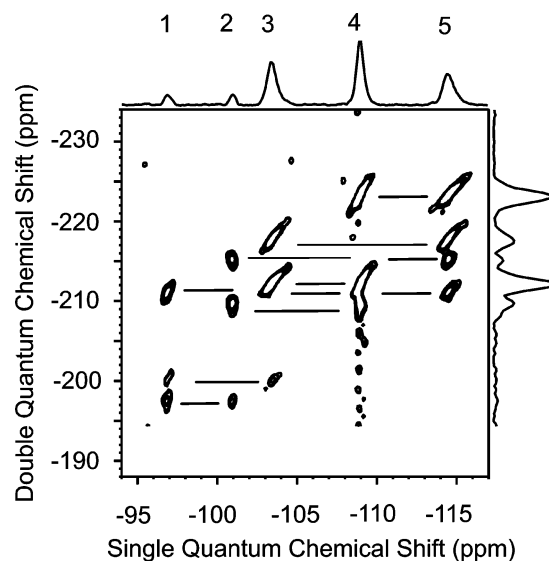


Figure 4. J -coupling-mediated 2D INADEQUATE $^{29}\text{Si}\{^{29}\text{Si}\}$ MAS NMR spectrum from a lamellar silicate- $\text{C}_{16}\text{N}^+\text{Me}_2\text{Et}$ mesophase with a molecularly ordered framework (see Figures 2 and 3). Projections of the spectrum accompany the contour plot along the horizontal single-quantum and vertical double-quantum dimensions. Proximities between pairs of J -coupled nearest-neighbor ^{29}Si T-sites are established by correlated ^{29}Si signal intensities at identical double-quantum chemical shifts. Systematic noise due to T_1 relaxation during the measurement is visible for the signal associated with site 4, due to the greater intensity of this signal relative to the others.

a cationic surfactant headgroup, which fulfills the 4-fold coordination of each T-site. Similarly, signal intensity in Figure 4 associated with Q^4 site 5 is correlated with four signals from sites 1, 2, 3, and 4, from which its full complement of four framework T-site interconnectivities is established. These results are confirmed by the separate dipole-dipole-mediated 2D double-quantum ^{29}Si MAS NMR spectrum in Figure 2: the most intense pairs of correlated signals result from dipole-dipole interactions between nearest-neighbor $^{29}\text{Si}-\text{O}-^{29}\text{Si}$ T-sites, consistent with the through-bond J -mediated $^{29}\text{Si}-\text{O}-^{29}\text{Si}$ interactions established in Figure 4.

The connectivities of Q^4 sites 3 and 4 require closer examination, but are also clearly established. J -coupling interactions unfortunately do not allow interconnectivities to be established between chemically equivalent ^{29}Si T-sites, such as between two different adjacent site-3 moieties. Nor can J -correlations be measured between T-sites that are more distant than nearest-neighbor $^{29}\text{Si}-\text{O}-^{29}\text{Si}$ moieties, because ^{29}Si J -coupling interactions are inherently weak. However, stronger through-space dipole-dipole interactions are sensitive to both. The dipole-dipole-mediated 2D DQ ^{29}Si MAS NMR spectrum of Figure 2 discussed above shows strong correlated signal intensities among nearest-neighbor sites 1, 2, and 5, in addition to other signals of substantially stronger or weaker intensity.

The significantly less-intense signals in Figure 2 arise from more weakly coupled, more distant T-sites, whereas the most intense signals arise from more strongly or multiply coupled sites. (No mobility differences exist between the different ^{29}Si moieties in the solid silicate framework.) Specifically, site 3 displays strong ^{29}Si DQ intensity correlations with sites 1 and 5, establishing each of these species to be nearest-neighbor framework moieties. Likewise, site 4 displays strong ^{29}Si DQ intensity correlations with sites 2 and 5. The very weak intensities that are observed for the 'diagonal' signals in the

Table 1. ^{29}Si NMR Dipole–Dipole Interaction Strengths (D) and Their Corresponding ^{29}Si –O– ^{29}Si Distances (r), as Determined from Spinning-Sideband Analyses of a 2D DQ ^{29}Si MAS NMR Spectrum^a

DQ coherence	D (Hz) ± 5 Hz	r (nm) ± 0.003 nm
4–5	186	0.297
3–5	195	0.292
3–4	201	0.290

^a For each DQ coherence, the sideband manifolds associated with each site in a given pair were analyzed separately, and the symmetric results were averaged; as indicated, the estimated uncertainties are small. The dipole–dipole interactions and distances can be determined only qualitatively for the Q^3 sites, because of their large and interfering chemical shift anisotropies.

2D DQ ^{29}Si NMR spectrum of Figure 2 furthermore indicate that there are no nearest-neighbor T-site connectivities between any identical sites (i.e., site 3 does not have another site-3 ^{29}Si as a nearest-neighbor T-site, nor does site 4 have another site-4 ^{29}Si as a nearest neighbor). This, and the fact that the interconnectivities of T-sites 1, 2, and 5 are fully specified, leads to only a single allowable framework configuration, namely that each Q^4 site 3 is connected to two site-4 moieties and similarly that each Q^4 site 4 is connected to two site-3 species. This is consistent with the correlated DQ ^{29}Si signals in Figure 2 between sites 3 and 4, which are twice as intense as for other nearest-neighbor T-sites (e.g., between sites 3 and 5).

^{29}Si NMR dipole–dipole interaction strengths (D) and their corresponding ^{29}Si –O– ^{29}Si distances (r) were independently determined for Q^4 sites 3, 4, and 5 to confirm that they are within the range anticipated for typical nearest-neighbor T-site moieties. Values for D and r ($D \propto r^{-3}$) were obtained from spinning-sideband-analyses¹⁴ of 2D DQ ^{29}Si MAS NMR spectra, in which dipole–dipole interactions were reintroduced under MAS conditions.⁴¹ As shown in Table 1, the ^{29}Si – ^{29}Si dipole–dipole coupling constants and distance measurements establish quantitatively that Q^4 sites 3 and 4 (as well as site 5) are separated by 0.29–0.30 nm, well within the range expected for adjacent ^{29}Si –O– ^{29}Si T-sites.

Thus, the nearest-neighbor interconnectivities among all five of the tetrahedrally coordinated silicate sites in the framework are unambiguously determined, as summarized in Table 2. For the two triply connected Q^3 moieties and three quadruply connected Q^4 moieties in the molecularly ordered silicate– $\text{C}_{16}\text{N}^+\text{Me}_2\text{Et}$ mesophase under consideration here, the total number of different interconnectivity patterns statistically could be as high as $18!/(3!3!4!4!4!) = 1.3 \times 10^{10}$ (most of which are not physically reasonable). On the basis of realistic Si–O–Si bond angles and distances, recent topological analyses have identified, for example, of order 10^3 different possible framework configurations for 3D crystalline networks comprised of three distinct tetrahedrally coordinated atomic sites.⁴² For the five-T-site (pentanodal) layered silicate structure under consid-

Table 2. Summary of Nearest-Neighbor Connectivities among the Five Different Tetrahedrally Coordinated Silicon Atom Sites in a Lamellar Silicate– $\text{C}_{16}\text{N}^+\text{Me}_2\text{Et}$ Mesophase with a Molecularly Ordered Framework^a

silicon T-Site	^{29}Si NMR isotropic chemical shift, ppm	Q^n -type ^c	connectivities to adjacent Si sites via bridging oxygen atoms
1	–97.0	Q^3	2, 3, and 5
2	–101.0	Q^3	1, 4, and 5
3	–103.7	Q^4	1, 5, and two different 4's
4	–109.1	Q^4	2, 5, and two different 3's
5	–114.7	Q^4	1, 2, 3, and 4

^a The connectivities are established by the strong intensity correlations shown in the 2D DQ ^{29}Si MAS NMR spectra of Figures 2 and 4. The sites are labeled '1' to '5' in a sequence of decreasing isotropic ^{29}Si NMR chemical shift.

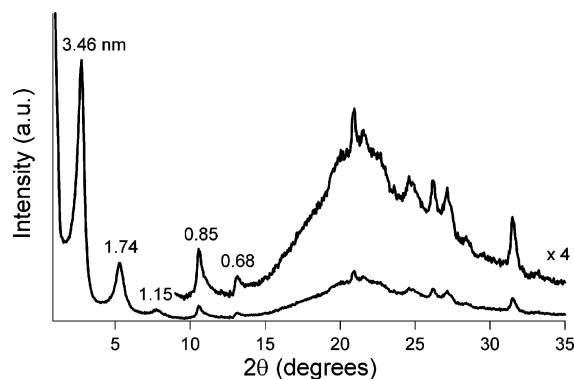


Figure 5. X-ray powder diffraction pattern from the molecularly ordered silicate– $\text{C}_{16}\text{N}^+\text{Me}_2\text{Et}$ mesophase material for which ^{29}Si NMR spectra are given in Figures 2–4. Diffraction peaks at 3.46, 1.74, and 1.15 nm correspond to the first three orders of diffraction from the layered mesophase structure, whereas those at 0.85 and 0.68 nm are attributed to the a - and b -axes of the silicate framework structure, respectively.

eration here, a substantially larger number of realistic topological possibilities exist. Out of the large number of possible configurations, the 2D DQ ^{29}Si NMR results nevertheless constrain the framework T-site interconnectivities to just a single set.

More subtle details of the framework structure are obtained from analyses of the less intense signal correlations in the dipole–dipole-mediated DQ ^{29}Si MAS NMR spectrum of Figure 2. The spectrum was acquired using a 1.6-ms double-quantum excitation time, such that the weak ‘diagonal’ intensity correlations each reflect *next*-nearest-neighbor ^{29}Si –O–Si–O– ^{29}Si proximities between two identical site-3, site-4, or site-5 ^{29}Si framework moieties. In addition, weak but distinct ‘off-diagonal’ intensity correlations are clearly observed between sites 1 and 4 and between sites 2 and 3. These constraints are crucial to the determination of the framework structure.

Mesoscopic and molecular order in the silicate– $\text{C}_{16}\text{N}^+\text{Me}_2\text{Et}$ mesophase are additionally evident from the XRD data shown in Figure 5. The small-angle regime shows three peaks with d -spacings of 3.46, 1.74, and 1.15 nm, corresponding to the first three orders of diffraction from the lamellar mesostructure. A number of sharp diffraction peaks can be seen at wider angles, which arise from the 2D molecular ordering of the silicate framework and the corresponding organization of surfactant molecules.¹ Temperature-dependent XRD experiments (data not shown) revealed that while the small-angle diffraction peaks due to the lamellar mesophase, (and several of the wide-angle peaks) shift markedly with temperature, many of the wide-angle peaks do not. In particular, those corresponding to d -spacings of 0.85 and 0.68 nm do not vary with temperature (in the range

(41) The intensities of the spinning sidebands that appear in 2D DQ ^{29}Si MAS NMR spectra depend on the strengths of the dipole–dipole interactions (D) between coupled spin pairs, as well as on MAS spinning speed and the number of excitation cycles applied during the recoupling process. With D constant and the MAS speed held constant, several mixing times with different excitation cycles were examined, which led to comparable values for D and r . Measurements made using shorter mixing times are less affected by influences from more distant and multiple ^{29}Si couplings, and thus tend to give more accurate results; a short mixing time (3.2 ms) was used to obtain the values reported in Table 1.

(42) Friedrichs, O. D.; Dress, A. W. M.; Huson, D. H.; Klinowski, J.; Mackay, A. L. *Nature* **1999**, *400*, 644–647.

from about $-30\text{ }^{\circ}\text{C}$ to $60\text{ }^{\circ}\text{C}$), indicating that they are associated with molecular ordering of the silicate framework. Comparison with the proposed framework structure (see below) suggests that these peaks correspond to the *a*- and *b*-axes of the silicate unit cell.

The XRD analysis of a 2D framework structure, in combination with the nearest- and next-nearest-neighbor T-site connectivities established by 2D DQ ^{29}Si NMR, greatly constrains the ways in which the five distinct tetrahedrally coordinated ^{29}Si sites can be arranged. To assess whether the NMR/XRD-derived framework interconnectivities are consistent with a stable and energetically preferred structure, quantum chemical simulations were performed, from which atomic coordinates were extracted. To do so, the Si connectivities among the five distinct T-sites in Table 2 were first converted into atomic positions on a two-dimensional crystal lattice with a formula unit of $\text{Si}_{10}\text{O}_{22}\text{H}_4$. Structural minimizations were then performed with both empirical force field¹⁰ and periodic ab initio methods,¹¹ using lattice coordinates that were fixed to those determined from the wide-angle XRD data (*a*- and *b*-axis spacings 0.85 and 0.68 nm, respectively, Figure 5) to ensure self-consistency. To preserve generality, these minimizations were carried out with no symmetry imposed (*P1*). Both approaches yielded very similar results, which are summarized in Table 3 as fractional coordinates of Si and O atoms in the layered sheet framework. In both cases, they demonstrate that the structure derived from the 2D DQ ^{29}Si NMR and XRD results is indeed stable with only minor refinements in atomic positions. Only one framework configuration was found to fit all of the constraints imposed by the NMR and XRD data.

The energy-minimized silicate framework structure thus obtained by quantum chemical modeling¹¹ is shown in Figure 1. Note that the $\sim 1.0\text{-nm}$ -thick silicate sheets have a combination of four- and six-membered silicate rings in a locally highly ordered open 2D framework. The four-membered ring in Figure 1b forms a rhombus with two site-4 Si atoms along the short diagonal and two site-3 Si atoms along the long diagonal. This is in notable agreement with the different correlated 2D DQ ^{29}Si NMR signal intensities observed along the diagonal in Figure 2: stronger next-nearest-neighbor ^{29}Si interactions are evident between two site-4 framework species, while interactions are weaker between nearby site-3 moieties. Furthermore, the terminal oxygen atoms associated with the Q^3 framework sites are directed outward toward the silicate–surfactant interfaces, where their negative charges are accessible to the strong structure-influencing interactions of the cationic $\text{C}_{16}\text{N}^+\text{Me}_2\text{Et}$ headgroups. The manner in which the $-\text{N}^+\text{Me}_2\text{Et}$ surfactant headgroups interact with and direct the silicate framework is under further study using neutron diffraction and NMR cross-polarization techniques. The presence of four- and six-membered silicate rings in the 2D crystalline framework is consistent with similar locally ordered structures that are formed in the presence of nonsurfactant cations or quaternary amines in solution and in the syntheses of 3D crystalline zeolites.^{43–45}

The resulting energy-minimized structure depicted in Figure 1 satisfies all of the double-quantum ^{29}Si NMR-interconnectivity

Table 3. Fractional Coordinates for the Molecularly Ordered Silicate Framework Structure of the Lamellar Silicate– $\text{C}_{16}\text{N}^+\text{Me}_2\text{Et}$ Mesophase^a

framework atom site	fractional coordinates		
	X	Y	Z
Si-1	0.2502	0.2675	0.0728
	0.9512	0.8816	0.8517
Si-2	0.9238	0.3240	0.1242
	0.2728	0.8241	0.7960
Si-3	0.7759	0.2328	0.9054
	0.4120	0.9144	0.0218
Si-4	0.4635	0.1490	0.8664
	0.7283	0.9981	0.0562
Si-5	0.8722	0.6114	0.9801
	0.3240	0.5348	0.9394
O-1	0.0901	0.8840	0.7894
	0.1111	0.2911	0.1351
O-2	0.9303	0.1092	0.8800
	0.2577	0.0292	0.0541
O-3	0.2108	0.3979	0.9945
	0.9927	0.7418	0.9269
O-4	0.4175	0.3359	0.1088
	0.7943	0.7995	0.8084
O-5	0.8414	0.1052	0.1179
	0.3703	0.0320	0.8003
O-6	0.9161	0.4593	0.0474
	0.2817	0.6929	0.8735
O-7	0.8415	0.4317	0.1962
	0.3167	0.7046	0.7192
O-8	0.6450	0.1804	0.8412
	0.5503	0.9534	0.0846
O-9	0.4498	0.0112	0.9405
	0.7209	0.1545	0.9875
O-10	0.7912	0.4694	0.9152
	0.4053	0.6764	0.0061
O-11	0.4106	0.3715	0.8867
	0.7810	0.7820	0.0270
H-1	0.8161	0.6933	0.7727
	0.4510	0.4712	0.1012
H-2	0.4016	0.6103	0.7169
	0.8540	0.5729	0.2017

^a The coordinates were derived from the 2D DQ ^{29}Si MAS NMR interconnectivity constraints, small- and wide-angle XRD data, and optimized by quantum-chemical energy minimization with a unit cell dimension of $\{a, b, c\} = \{0.85, 0.68, 1.75\}$ nm, average Si–O distance = 0.163 nm, standard deviation = 0.002 nm.

and XRD constraints. Furthermore, based on the local T-site bonding configurations in the framework, separate ab initio predictions can be made of the expected isotropic ^{29}Si chemical shifts for the different T-sites as an independent verification of self-consistency. These calculations make use of recent computational and theoretical advances that enable detailed quantitative analyses of the effects of local electron density on NMR signals. They have been used, for example, to examine and predict isotropic chemical shifts for different bonding geometries in crystalline solids.²¹ Table 4 shows the predicted isotropic ^{29}Si chemical shifts associated with each T-site in the energy minimized framework structure (Figure 1), along with the experimentally determined ^{29}Si isotropic chemical shifts and CSA tensor elements. Comparison of the independently predicted and experimentally measured ^{29}Si isotropic chemical shifts shows them to be in reasonable agreement. Careful inspection of the structure shows that it has 10 different Si-atom T-sites, with an inversion center that places it in the space group $P\bar{1}$. The five resolved peaks in the experimental ^{29}Si MAS NMR spectrum (Figure 2) and the closely spaced pairs of peaks (Table 4) with similar isotropic ^{29}Si chemical shifts in the calculated MAS spectrum, indicate that the structure has nearly

(43) Szostak, R. *Molecular Sieves Principles of Synthesis and Identification*; Van Nostrand Reinhold: New York, 1989.

(44) Engelhardt, G.; Michel, D. *High-Resolution Solid-State NMR of Silicates and Zeolites*; John Wiley and Sons: Chichester, 1987.

(45) Harris, R. K.; Knight, C. T. *J. Mol. Struct.* **1982**, *78*, 273–278.

Table 4. Experimental and Predicted ^{29}Si Isotropic Chemical Shifts (σ_{iso}) and Experimentally Determined Chemical Shift Tensor Elements $\{\sigma_{11}, \sigma_{22}, \sigma_{33}\}$ for the Molecularly Ordered Silicate Framework Structure of the Lamellar Silicate- $\text{C}_{16}\text{N}^+\text{Me}_2\text{Et}$ Mesophase^a

framework site ^b	predicted σ_{iso} ^{29}Si (ppm)	experimental σ_{iso} ^{29}Si (ppm)	experimental chemical shift tensor elements $\{\sigma_{11}, \sigma_{22}, \sigma_{33}\}$ ^{29}Si (ppm)
Si-1	-91.2	-97.0	{-156, -71, -61}
Si-1*	-88.4		
Si-2	-99.0	-101.0	{-144, -83, -73}
Si-2*	-99.4		
Si-3	-100.8	-103.7	{-112.5, -98.5, -98.5}
Si-3*	-102.4		
Si-4	-109.0	-109.1	
Si-4*	-108.0		
Si-5	-111.7	-114.7	
Si-5*	-110.3		

^a The predicted ^{29}Si isotropic chemical shifts were calculated for the energy minimized structure (Figure 1), whose fractional coordinates are shown in Table 3, by using density functional theory with periodic boundary conditions.^{20,21} ^b Chemical shift calculations yield pairs of closely spaced peaks (e.g., Si-1 and Si-1*) that appear to be equivalent within the resolution limits of the NMR measurements.

2-fold symmetry, within the resolution limits of the NMR measurements. Interestingly, the slanted elliptical intensity correlations that are evident in the 2D DQ ^{29}Si NMR spectra of both Figures 2 and 4 reflect even greater extents of local ordering³⁵ between certain T-site pairs (e.g., 3-4, 3-5, and 4-5), than indicated by the ~ 1 -ppm line widths of the 1D ^{29}Si MAS spectrum and projections. Further work is underway to establish and clarify the nature of these subtle and surprisingly rich local structural features.

Conclusions

The molecularly ordered intraframework structure of a novel non-3D-crystalline lamellar silicate- $\text{C}_{16}\text{NMe}_2\text{Et}^+$ surfactant mesophase has been self-consistently determined by 2D DQ ^{29}Si NMR, in conjunction with small- and wide-angle X-ray diffraction, quantum chemical calculations, and modeling with empirical force fields. The resulting zeolite-like 2D silicate framework structure consists of five equally populated tetrahedrally coordinated silicon sites that form four- and six-

membered-ring moieties, which are linked together in contiguous 2D sheets that are approximately 1.0 nm thick. The structure is energetically stable, as confirmed by modeling. Independent predictions of isotropic ^{29}Si chemical shifts, based on the geometries (bond angles and distances) of lattice T-sites, yield self-consistent results. These findings establish that the cationic surfactant headgroups direct molecular framework ordering in a manner that is apparently analogous to the role of organic cations in zeolite syntheses, forming unusual open 2D silicate sheets. The combination of 2D J -coupling (through-bond) and 2D dipole-dipole-coupling (through-space) DQ ^{29}Si NMR measurements, in conjunction with quantum chemical modeling and X-ray diffraction, captures key and subtle characteristics of the novel two-dimensionally ordered framework structure of this lamellar silicate-surfactant mesophase. These results represent a new way to establish the framework structures of partially ordered, semicrystalline, or heavily defected solids. Such an approach is expected to have broad impact on many technologically important materials, such as surfactant-templated inorganic solids, proteins, polymers, and nanocrystals, whose high extents of often short-range molecular ordering would otherwise be indeterminate.

Acknowledgment. We thank Dr. V. Breedveld, Dr. E. Flanigen, Dr. A. J. Levine, and Dr. S. Zones for helpful discussions, Dr. N. Henson for assistance with the VASP and GULP computations, and Dr. M. Profeta, Dr. F. Mauri, and Dr. C. J. Pickard for providing us with their NMR prediction module and for assistance with the PARATEC code. Calculations were performed at LANL and at the IDRIS supercomputer center of the CNRS. This work was supported by the USARO through MURI grant DAAH04-96-1-0443 and by the UCSB Materials Research Laboratory under award DMR-00-80034. A NATO Collaborative Research Grant is gratefully acknowledged. N.H. thanks the STINT Foundation and the Stiftelsen Blanceflor Boncompagni-Ludovisi född Bildt for postdoctoral fellowships. R.C.H. is a recipient of an NSF Graduate Research Fellowship.

JA040030S